Extended Abstracts of the 2009 International Conference on Solid State Devices and Materials, Sendai, 2009, pp254-255

J-2-6

Investigation of strained-Sb Hetrostructures with high hole mobility

Aneesh Nainani*, Masaharu Kobayashi, Daniel Witte, Toshifumi Irisawa, Tejas Krishnamohan and Krishna Saraswat
*Center for Integrated Systems, Department of Electrical Engineering, Stanford University, CA 94305 *nainani@stanford.edu*
Brian R. Bennett**, Mario G. Ancona and J. Brad Boos
*Naval Research Laboratory, Washington, DC 20375 **brian.bennett@nrl.navy.mil*

Background: III-V semiconductors are one of the most promising device candidates for future high-speed, low-power logic applications due to their high electron mobility. Recently, high performance III-V n-FETs have been demonstrated [1]. However, for CMOS logic, there is a significant challenge of identifying high mobility III-V p-FET candidates [2]. Biaxial strain can be easily introduced in III-V hetrostructures during MBE growth. Biaxial strain splits the degeneracy between light hole (*lh*) & heavy hole (*hh*) bands reducing the transport effective mass (m*) and number of states available for interband scattering thereby enhancing hole mobility (μ_h). Percentage of strain induced (%), Valence Band Offset (VBO) for confining the 2 Dimensional Hole Gas (2DHG), modulation doping, dominant scattering limiting μ_h , reduction of m* with strain are some of the parameters that need to be investigated for achieving high hole mobilities in III-V's.

Introduction: In this paper we first use modeling to compare μ_h and its enhancement with strain in As's and Sb's. Sb hetrostructures based on two different approaches are analyzed. Strain is quantified using high resolution XRD analysis, XPS analysis is used to estimate VBO's. Temperature Dependent Hall measurements are performed to identify the dominant scattering mechanisms. Finally effective mass (m*) and its reduction with strain is quantified using Shubninov-de Haas oscillations.

Modeling: Band Structure using 8 band k.p [2] + Kubo-greenwood approach is used to calculate μ_h in $In_xGa_{1-x}As$ and $In_xGa_{1-x}Sb$ (Sheet Charge (N_S) $=10^{12}/cm^2$). Sb's have ~2X higher μ_h than As's (Fig. 1(inset)). Enhancement with biaxial strain is calculated using 8x8 Hamiltonian with Spin Orbit coupling [2]. We observe compression is better than tension (Fig. 1) & % mobility enhancement with strain is similar for As's & Sb's (~2.2X with 2% compression). But strained Sb's have much higher mobilities due to their higher unstrained mobility values. Sb channels with biaxial compression are optimal for achieving high μ_h.

Hetrostructure Design & Details: Looking at the Bandedges vs. Lattice constants (Fig. 2) there can be 2 possible approaches for achieving biaxial compression in Sb channels i.e (A) using $In_xGa_{1-x}Sb$ channel and $Al_yGa_{1-y}Sb$ barrier. Compression in high Ga%, $In_xGa_{1-x}Sb$ channel is not possible using this approach & the maximum VBO is ~0.39eV. Approach (B) uses binary GaSb channel with $AlAs_xSb_{1-x}$. This gives a higher VBO for confining the 2DHG & use of a binary channel avoids alloy scattering. We investigate Hetrostructures with $In_{0.41}GaSb$ channels (approach A) and GaSb channels (approach B) grown using MBE on semi-insulating GaAs (100) substrate (Fig. 3). The $AlAs_xSb_{1-x}$ for approach B is grown as superlattice of AlAs & AlSb [3]. Table 4 lists the samples investigated, details of the growth procedures are summarized in [3-4]. $In_{0.41}GaSb$ channels are modulation-doped with Be after channel growth and GaSb channels are modulation-doped with Be prior to channel growth (Fig. 3).

Strain: High resolution XRD analysis is used to quantify strain. Fig. 4 shows the rocking XRD curves near the (004) GaAs peak for sample A1 ($In_{0.41}GaSb$ channel) & sample B1 (GaSb channel with superlattice of $(AlAs)_xAlSb_{1-x}$). For sample A1 (Fig. 4 (a)) peaks are visible for the InGaSb channel, AlGaSb barrier and the GaAs substrate. For sample B1 (Fig. 4 (a)) we see the main and satellite peaks for the digital superlattice (n=-1,0,and+1), the 100nm AlSb buffer layer and the GaAs substrate (Fig. 4(b)). The GaSb channel peak gets buried in the satellite peak from the superlattice. Thickness for the AlSb & AlAs are determined by matching the XRD results with simulations and the $AlAs_xSb_{1-x}$ ternary composition is calculated using Vegard's law; Table 1 summarizes the results. Complete relaxation for the superlattice & the 100nm AlSb layer yields a good match to the peak position in the rocking curve, this is further confirmed by a reciprocal lattice scan around the (004) & (115) reciprocal lattice points (Fig. 5). The epilayer peaks are all broadened compared to the simulation. This is a result of a high density of misfit dislocations required to relax the high 7-8% lattice mismatch with substrate.

VBO: Citric acid based etch is used to selectively remove the InAs capping layer, a HCl solution based timed etch is then used to etch the subsequent Sb layers (Fig. 3). VBO is calculated (Fig. 6) by taking the difference between VB spectrum from channel and barrier (~0.3eV for A1 and ~0.6eV for B1). Ga 3d & In 4d peaks are used for reference. SbO_x formation & Sb accumulation on the surface after etching is also observed and will be discussed elsewhere. Higher VBO is achieved using the $AlAs_xSb_{1-x}$ barrier (approach B) as compared with $In_yAl_{1-y}Sb$ (approach A).

μ_h: Hall measurements are performed on the samples varying temperature from 2K-300K. Fig. 7 summarizes the μ_h & N_S values. For samples A1, A2 & B1 a $T^{-3/2}$ temperature dependence in μ_h , characteristic of polar optical scattering (which is the dominant mechanism limiting hole mobility at room temperature (RT) [5]) is seen from 200-300K. In GaSb sample B1, a $T^{-1/2}$ temperature dependence characteristic of piezoelectric scattering (dominant in GaSb at low temperatures [5]) is also seen from 100-200K. Sample B2, B3 exhibit lower RT μ_h & maximum μ_h and a T^{-1} temperature dependence characteristic of mobility limited by interface defects [5]. N_S vs. T is fairly constant as expected in modulation doping. Sample B2 and B3 exhibit slight N_S freeze out at low T again suggesting poor interface/dislocation as a result of strain relaxation in these samples. μ_h saturates to a maximum value at low temperature in A1, A2 (modulation doped from top) while a dip in mobility at low temperature is seen in sample B1-B3 (modulation doped from bottom) due to dopant diffusion in the channel in latter samples causing columbic scattering.

m*: Shubnikov-de Haas (SdH) oscillations (Fig. 8) are observed in samples A1, A2 & B1 at low temperature (2-20K) and high magnetic fields (0-9 Tesla) confirming good crystal & interface quality while no oscillations are seen in B2 & B3. Effective mass is extracted from the temperature dependence of SdH oscillations [6]. Table. 2 summarizes the results: m* in bulk $In_{0.41}GaSb$ & GaSb, results from modeling & m_{min}* when the *lh* and *hh* become completely non-interacting are also listed for comparison. Results from SdH are confirmed using Cyclotron resonance in sample A1.

Summary: Maximum mobility of $980cm^2/Vs$ at RT ($N_S=1.2x10^{12}/cm^2$) is achieved. Strain results in significant reduction of m*. RT μ_h is limited by interface scattering when strain gets relaxed & polar optical scattering otherwise

[1]B. R. Bennett et. al. Solid-State Electron. 49,1875 [2]A.T.B. Bahder et. al., PR-B, 41, 11992 [3]B. R. Bennett et. al. J Cryst Growth, 311, 47. [4]B. R. Bennett et al, APL, 91, 042104 [5]J. D. Wiley, Semiconductor and Semimetals, 10, 91 [6]T.E. Whall et. al, APL, 64, 357

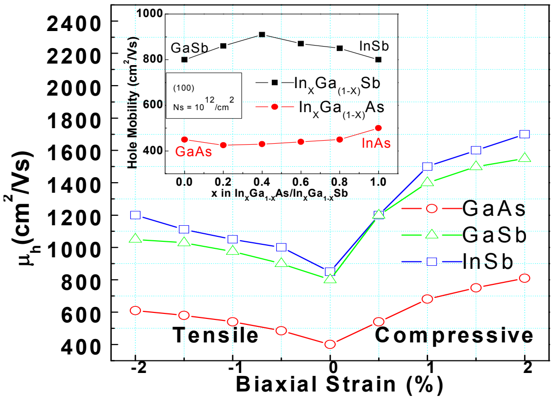

Fig.1. Mobility (μ_h) enhancement with biaxial strain (inset) Calculated μ_h for $In_xGa_{1-x}Sb$ & $In_xGa_{1-x}As$.

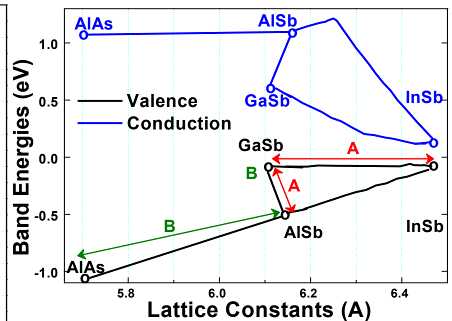

Fig.2 Two approaches for compressively strained Sb channel : (**A**) using $In_xGa_{1-x}Sb$ channel & $Al_yGa_{1-y}Sb$ barriers. (**B**) GaSb channel & $AlAs_xSb_{1-x}$ (superlattice of $(AlAs)_xAlSb_{1-x}$) as barrier (see text).

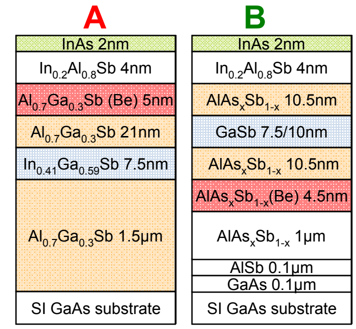

Fig.3. Hetrostructures based on approaches (**A**) & (**B**). Growth details in [3-4]

Sample	Channel	Barrier	Strain (%)	VBO (eV)	Ns(cm^{-2}) (300K)	μ_h (cm^2/Vs) (300K)	μ_{max} (cm^2/Vs)
A1	$In_{.41}Ga_{.59}Sb$ (75Å)	$Al_{0.7}Ga_{0.3}Sb$	1.85	0.3	$1.2x10^{12}$	960	4500
A2	$In_{.41}Ga_{.59}Sb$ (75Å)	AlSb	2.0	0.39	$9x10^{11}$	900	5000
B1	GaSb (75Å)	$AlAs_{0.22}Sb_{0.78}$	1.06	0.56	$1.75x10^{12}$	880	4400
B2	GaSb (75Å)	$AlAs_{0.24}Sb_{0.76}$	1.48	0.58	$1.60x10^{12}$	690	1500
B3	GaSb (100Å)	$AlAs_{0.27}Sb_{0.73}$	1.22	0.6	$1.85x10^{12}$	600	1000

Table.1:Summary of samples.

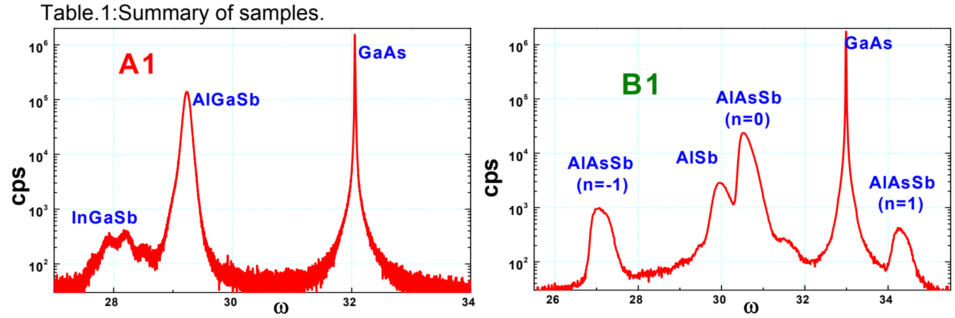

Fig.4. High Resolution XRD scans on the samples A1 (left) & B1 (right) near (004) GaAs peak.

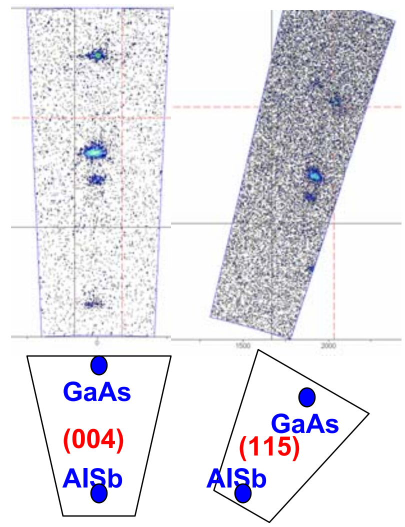

Fig.5. Reciprocal Lattice scan on sample A1 around (0 0 4) left & (1 1 5) right.

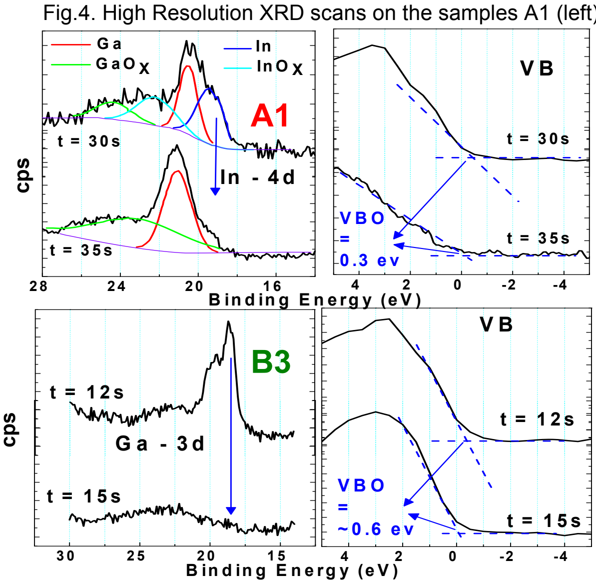

Fig 6. VBO offsets are estimated using high resolution XPS (Sample : A1 (top), B3 (bottom))

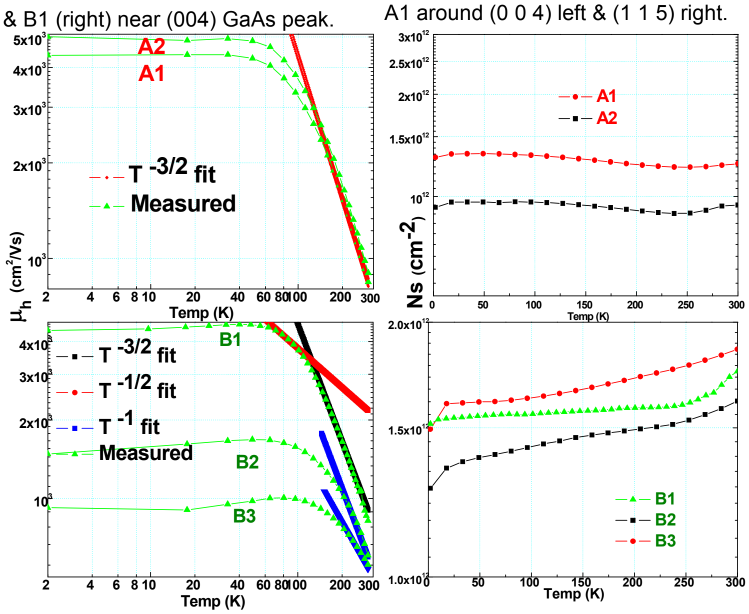

Fig 7. μ_h and N_S as function of Temp. for sample A1-A2 (top) & B1-B3 (bottom).

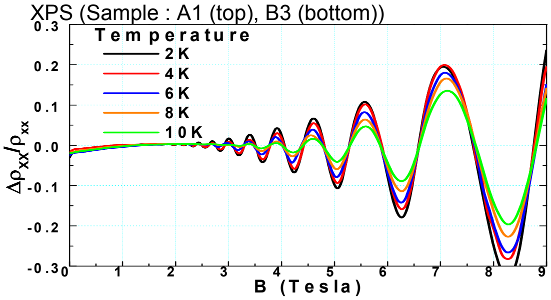

Fig.8. Temp dependence of Shubnikov-de Hass oscillations (above : A1) is used to calculate m*

Sample	Channel	Strain (%)	m*
Bulk	$In_{.41}Ga_{.59}Sb$	0	0.40
A1	$In_{.41}Ga_{.59}Sb$	1.85	0.099 ± 0.02 (**SdH**), 0.09 (**k.p**)
A2	$In_{.41}Ga_{.59}Sb$	2.0	0.0946 ± 0.01 (**SdH**), 0.085 (**k.p**) 0.096 (**Cyclotron resonance**)
Max	$In_{.41}Ga_{.59}Sb$	Maximum	0.06 (**k.p = 1/(γ1+ γ2)**)
Bulk	GaSb	0	0.35
B2	GaSb	1.06	0.12 (**SdH**), 0.1 (**k.p**)
Max	GaSb	Maximum	0.07 (**k.p = 1/(γ1+ γ2)**)

Table.2: m* with strain : Extracted value from oscillations (**SdH**), results from modeling (**k.p**) & verification with **Cyclotron resonance**